A Time-Varying-Constrained Motion Generation Scheme for Humanoid Robot Arms

Zhijun Zhang(✉), Lingdong Kong(✉), and Yaru Niu

School of Automation Science and Engineering,
South China University of Technology, Guangzhou 510641, China
auzjzhang@scut.edu.cn, scutkld@foxmail.com

Abstract. An efficient time-varying gesture-determined dynamical (TV-GDD) scheme is proposed for motion planning of redundant dual-arms manipulation. Motion planning for such tasks on humanoid robots with a high number of degrees-of-freedom (DOF) requires computationally efficient approaches to generate the expected joint configuration when given the end-effector tasks. To do so, we investigate a time-varying joint-limits constrained quadratic-programming (QP) approach and an efficient numerical computing method. This strategy provides feasible solutions at a low computation cost within physical limits. In addition, the joint configuration can be adjusted dynamically according to the expected gestures and tasks. Comparative simulations and experimental results on a humanoid robot demonstrate the effectiveness and feasibility of the scheme.

Keywords: Humanoid robot · Dual arms · Motion generation
Quadratic programming · Redundancy resolution

1 Introduction

Humanoid robots can help people immerse themselves in environments of peer-to-peer cooperation and are thus increasingly welcomed in various applications [1]. Dual-arms of humanoid robots can not only fulfill manipulation tasks [2], but also perform important components of the body language [3]. In contrast to the single-arm system, multi-arm systems can be more efficient by performing motions simultaneously [4]. The early multi-arm system can trace back to Goertz's remote manipulators for handling of radioactive goods in the 1940's [5]. From the late 1950's to the early 1970's, dual-arms teleoperation was developed because of the deep-sea and deep-space exploration [6].

In recent years, due to the fast development of humanoid robots [2], dual-arm applications attract researchers and engineers' interests again. Humanoid robots require dual-arms to perform daily work naturally in home environment autonomously or semi-autonomously [7]. They can also improve the sociability with displaying emotional body language [8]. To perform daily tasks with

T. Huang et al. (Eds.): ISNN 2018, LNCS 10878, pp. 757–767, 2018.
https://doi.org/10.1007/978-3-319-92537-0_86

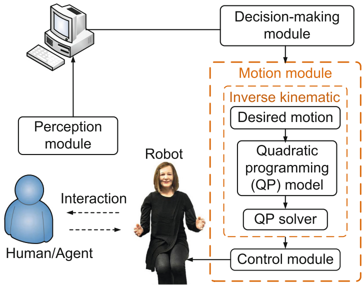

Fig. 1. System architecture of the female humanoid robot.

dual-arms of humanoid robots, the dual-arms motion planning should be considered. One of the basic problems is the inverse kinematic problem. Nunez *et al.* presented an analytic solution to humanoid robot arms [9], of which each arm has three DOF. However, most humanoid robot arms in actual applications have more DOF and are thus redundant. This redundancy improves the flexibility when the robot implement end-effector tasks [10], and inevitably increases computation difficulties. Traditional redundancy-resolution methods are pseudoinverse-based schemes. Wang and Li proposed a closed-loop inverse kinematics based on pseudoinverse method, which is used to dual-arms on a mobile platform [10]. Note that the above methods have to compute the matrix inverse, then QP methods are preferred recently. Kanoun *et al.* proposed a QP-based task priority framework to resolve the kinematic-redundancy problem [11]. Zhang and Zhang performed QP-based methods on a physical planar manipulator [12]. To solve the redundant-resolution problem effectively, two redundancy-resolution schemes are presented and their equivalence relationship was proved [13]. However, most existing optimization methods focus on a single manipulator, and only a few consider dual-arms of humanoid robots [11]. Inspired by the above works, a QP-based online generation scheme is proposed in this paper to generate expected gestures of dual-arms. The gestures are movements or positions of the hand, arm, body which express idea, intention, opinion, emotion, etc. To obtain the optimization solutions of the designed QP scheme, a discrete numerical method is presented to control the robot to finish not only tasks of end-effectors but also some expected subtasks. The architecture of this system is shown in Fig. 1. It allows an easier coordination of interaction between two arms. Before ending this section, the main contributions of this paper are as follows:

- A time-varying gesture-determined dynamical (TV-GDD) scheme for dual-arms coordinated motion generation is proposed and applied to an actual humanoid robot.
- Different from the pseudoinverse methods or QP-based methods focusing on single or planar dual arms, together with the numerical QP solver, the proposed TV-GDD scheme can on-line generate behaviors for humanoid robots.

- To enable generating expected arm configurations, a novel TV-GDD function is designed, proposed and discussed in details, which can make the arms move according to the expected gesture.

2 General Quadratic Programming Model

The presented robot in this paper is a humanoid robot with a sitting posture. It is able to display realistic facial and body expressions. It has two arms and the dual arms have 14 DOF (7 of each arm). The origin of Frame {0} is chosen at the waist (i.e., the base). The forward kinematics of the dual arms is that given the left/right joint-space vectors θ_{L} and θ_{R}, the end-effector position vectors r_{L} and r_{R} can be obtained as follows:

$$r_{\mathrm{L}} = f_{\mathrm{L}}(\theta_{\mathrm{L}}),\ r_{\mathrm{R}} = f_{\mathrm{R}}(\theta_{\mathrm{R}}) \tag{1}$$

where $f_{\mathrm{L}}(\cdot)$ and $f_{\mathrm{R}}(\cdot)$ are smooth nonlinear functions. Generally, Eq. (1) can be obtained when the structure of the robot is known. One fundamental issue for redundant robots is the inverse kinematics problem, i.e., to obtain the joint vectors with given end-effector trajectories.

The classical approaches to solving the redundancy-resolution problem are pseudoinverse methods. Specifically, at the joint-velocity level, the pseudoinverse type solution can be formulated as

$$\dot{\theta}_{\mathrm{L}} = \mathcal{J}_{\mathrm{L}}^{\dagger}(\theta_{\mathrm{L}})\dot{r_{\mathrm{L}}} + (\mathcal{I} - \mathcal{J}_{\mathrm{L}}^{\dagger}(\theta_{\mathrm{L}})\mathcal{J}_{\mathrm{L}}(\theta_{L}))w_{\mathrm{L}} \tag{2}$$

$$\dot{\theta}_{\mathrm{R}} = \mathcal{J}_{\mathrm{R}}^{\dagger}(\theta_{\mathrm{R}})\dot{r_{\mathrm{R}}} + (\mathcal{I} - \mathcal{J}_{\mathrm{R}}^{\dagger}(\theta_{\mathrm{R}})\mathcal{J}_{\mathrm{R}}(\theta_{\mathrm{R}}))w_{\mathrm{R}} \tag{3}$$

where $\mathcal{J}_{\mathrm{L}}^{\dagger}(\theta_{\mathrm{L}}) \in \mathbb{R}^{n\times m}$ and $\mathcal{J}_{\mathrm{R}}^{\dagger}(\theta_{\mathrm{R}}) \in \mathbb{R}^{n\times m}$ denote the pseudoinverse of the Jacobian matrices $\mathcal{J}_{\mathrm{L}}(\theta_{\mathrm{L}})$ and $\mathcal{J}_{\mathrm{R}}(\theta_{\mathrm{R}})$; $\mathcal{I} \in \mathbb{R}^{n\times n}$ is the identity matrix; $w_{\mathrm{L}} \in \mathbb{R}^{n}$ and $w_{\mathrm{R}} \in \mathbb{R}^{n}$ are arbitrary vectors selected for optimization criteria.

The traditional pseudoinverse approaches (2)-(3) need to compute inverse matrices and do not properly consider the inequality problems [12]. Inspired by the previous work [13,14], an online optimization technique which resolve the redundancy problem is designed as follows:

(1) QP-based left and right arm schemes are exploited and formulated as

$$\begin{aligned}
\text{minimize}\quad & \dot{\theta}_{\mathrm{L}}^{\mathrm{T}}\mathcal{Q}\dot{\theta}_{\mathrm{L}}/2 + b_{L}^{T}\theta_{\mathrm{L}} && (4)\\
\text{subject to}\quad & \mathcal{J}_{\mathrm{L}}(\theta_{\mathrm{L}})\dot{\theta}_{\mathrm{L}} = \dot{r}_{\mathrm{L}} + \mathcal{K}_{\mathrm{L}}(r_{\mathrm{L}} - f_{\mathrm{L}}(\theta_{\mathrm{L}})) && (5)\\
& \theta_{\mathrm{L}}^{-} \leqslant \theta_{\mathrm{L}} \leqslant \theta_{\mathrm{L}}^{+} && (6)\\
& \dot{\theta}_{\mathrm{L}}^{-} \leqslant \dot{\theta}_{\mathrm{L}} \leqslant \dot{\theta}_{\mathrm{L}}^{+} && (7)
\end{aligned}$$

$$\begin{aligned}
\text{minimize}\quad & \dot{\theta}_{\mathrm{R}}^{\mathrm{T}}\mathcal{W}\dot{\theta}_{\mathrm{R}}/2 + b_{\mathrm{R}}^{\mathrm{T}}\theta_{\mathrm{R}} && (8)\\
\text{subject to}\quad & \mathcal{J}_{\mathrm{R}}(\theta_{\mathrm{R}})\dot{\theta}_{\mathrm{R}} = \dot{r}_{\mathrm{R}} + \mathcal{K}_{\mathrm{R}}(r_{\mathrm{R}} - f_{\mathrm{R}}(\theta_{\mathrm{R}})) && (9)\\
& \theta_{\mathrm{R}}^{-} \leqslant \theta_{\mathrm{R}} \leqslant \theta_{\mathrm{R}}^{+} && (10)\\
& \dot{\theta}_{\mathrm{R}}^{-} \leqslant \dot{\theta}_{\mathrm{R}} \leqslant \dot{\theta}_{\mathrm{R}}^{+} && (11)
\end{aligned}$$

where $\mathcal{Q} \in \mathbb{R}^{n\times n}$ and $\mathcal{W} \in \mathbb{R}^{n\times n}$ are coefficients of the quadratic terms; while b_{L} and b_{R} are those pertaining to the linear terms; $\mathcal{J}_{\mathrm{L}}$ and $\mathcal{J}_{\mathrm{R}}$ are the Jacobian matrices of the left/right arms, defined as $\mathcal{J} = \partial f(\theta)/\partial\theta$. Eqs. (5) and (9) express linear relations between the left/right end-effector velocities $\dot{r}_{\mathrm{L}} \in \mathbb{R}^m$ and $\dot{r}_{\mathrm{R}} \in \mathbb{R}^m$, and joint velocities $\dot{\theta}_{\mathrm{L}} \in \mathbb{R}^n$ and $\dot{\theta}_{\mathrm{R}} \in \mathbb{R}^n$; $\mathcal{K}_{\mathrm{L}}(r_{\mathrm{L}} - f_{\mathrm{L}}(\theta_{\mathrm{L}}))$ and $\mathcal{K}_{\mathrm{R}}(r_{\mathrm{R}} - f_{\mathrm{R}}(\theta_{\mathrm{R}}))$ are position-error feedbacks, where $\mathcal{K}_{\mathrm{L}}$ and $\mathcal{K}_{\mathrm{R}}$ are positive-definite symmetric (typically diagonal) $m \times m$ feedback-gain matrices. Eqs. (6) and (10) are bound constraints of joint-angle limits. Eqs. (7) and (11) are bound constraints of joint-velocity limits.

(2) To solve the above two QP problems simultaneously, (4)-(11) should be converted to a standard QP form. The criteria (4) and (8) are integrated as

$$\text{minimize} \begin{bmatrix} \dot{\theta}_{\mathrm{L}} \\ \dot{\theta}_{\mathrm{R}} \end{bmatrix}^{\mathrm{T}} \begin{bmatrix} W & \mathbf{0}_{n\times n} \\ \mathbf{0}_{n\times n} & Q \end{bmatrix} \begin{bmatrix} \dot{\theta}_{\mathrm{L}} \\ \dot{\theta}_{\mathrm{R}} \end{bmatrix} + \begin{bmatrix} b_{\mathrm{L}} \\ b_{\mathrm{R}} \end{bmatrix}^{\mathrm{T}} \begin{bmatrix} \dot{\theta}_{\mathrm{L}} \\ \dot{\theta}_{\mathrm{R}} \end{bmatrix}. \tag{12}$$

(3) Forward kinematics equations of left and right arms (5) and (9) are combined together as

$$\begin{bmatrix} \mathcal{J}_{\mathrm{L}} & \mathbf{0}_{3\times 7} \\ \mathbf{0}_{3\times 7} & \mathcal{J}_{\mathrm{R}} \end{bmatrix} \cdot \begin{bmatrix} \dot{\theta}_{\mathrm{L}} \\ \dot{\theta}_{\mathrm{R}} \end{bmatrix} = \begin{bmatrix} \dot{r}_{\mathrm{L}} \\ \dot{r}_{\mathrm{R}} \end{bmatrix} + \begin{bmatrix} k_{\mathrm{L}}(r_{\mathrm{L}} - f_{\mathrm{L}}(\theta_{\mathrm{L}})) \\ k_{\mathrm{R}}(r_{\mathrm{R}} - f_{\mathrm{R}}(\theta_{\mathrm{R}})) \end{bmatrix} \in \mathbb{R}^{2m\times 2n}. \tag{13}$$

(4) Joint-angle and joint-velocity limits of left and right arms (6) and (10) are combined as

$$\begin{bmatrix} \theta_{\mathrm{L}}^- \\ \theta_{\mathrm{R}}^- \end{bmatrix} \leqslant \begin{bmatrix} \theta_{\mathrm{L}} \\ \theta_{\mathrm{R}} \end{bmatrix} \leqslant \begin{bmatrix} \theta_{\mathrm{L}}^+ \\ \theta_{\mathrm{R}}^+ \end{bmatrix} \in \mathbb{R}^{2n}, \ \begin{bmatrix} \dot{\theta}_{\mathrm{L}}^- \\ \dot{\theta}_{\mathrm{R}}^- \end{bmatrix} \leqslant \begin{bmatrix} \dot{\theta}_{\mathrm{L}} \\ \dot{\theta}_{\mathrm{R}} \end{bmatrix} \leqslant \begin{bmatrix} \dot{\theta}_{\mathrm{L}}^+ \\ \dot{\theta}_{\mathrm{R}}^+ \end{bmatrix} \in \mathbb{R}^{2n}. \tag{14}$$

(5) Hence, the QP formulations (4)-(7) and (8)-(11) can be reformulated as

$$\text{minimize } \dot{\vartheta}^{\mathrm{T}}\mathcal{M}\dot{\vartheta}/2 + b^{\mathrm{T}}\vartheta \tag{15}$$
$$\text{subject to } \jmath(\vartheta)\dot{\vartheta} = \dot{\Upsilon} + \mathcal{K}(\Upsilon - f(\vartheta)) \tag{16}$$
$$\vartheta^- \leqslant \vartheta \leqslant \vartheta^+ \tag{17}$$
$$\dot{\vartheta}^- \leqslant \dot{\vartheta} \leqslant \dot{\vartheta}^+ \tag{18}$$

where $\vartheta = [\theta_{\mathrm{L}}^{\mathrm{T}}; \theta_{\mathrm{R}}^{\mathrm{T}}]^{\mathrm{T}} \in \mathbb{R}^{2n}$; $b = [b_{\mathrm{L}}^{\mathrm{T}}; b_{\mathrm{R}}^{\mathrm{T}}]^{\mathrm{T}}$; $\vartheta^- = [\theta_{\mathrm{L}}^{-\mathrm{T}}, \theta_{\mathrm{R}}^{-\mathrm{T}}]^{\mathrm{T}} \in \mathbb{R}^{2n}$; $\vartheta^+ = [\theta_{\mathrm{L}}^{+\mathrm{T}}, \theta_{\mathrm{R}}^{+\mathrm{T}}]^{\mathrm{T}} \in \mathbb{R}^{2n}$; $\dot{\vartheta} = \mathrm{d}\vartheta/\mathrm{d}t = [\dot{\theta}_{\mathrm{L}}^{\mathrm{T}}, \dot{\theta}_{\mathrm{R}}^{\mathrm{T}}]^{\mathrm{T}} \in \mathbb{R}^{2n}$; $\dot{\vartheta}^- = [\dot{\theta}_{\mathrm{L}}^{-\mathrm{T}}, \dot{\theta}_{\mathrm{R}^{-\mathrm{T}}}]^{\mathrm{T}} \in \mathbb{R}^{2n}$; $\dot{\vartheta}^+ = [\dot{\theta}_{\mathrm{L}}^{+\mathrm{T}}, \dot{\theta}_{\mathrm{R}}^{+\mathrm{T}}]^{\mathrm{T}} \in \mathbb{R}^{2n}$; $\dot{\Upsilon} = [\dot{r}_{\mathrm{L}}^{\mathrm{T}}; \dot{r}_{\mathrm{R}}^{\mathrm{T}}]^{\mathrm{T}} \in \mathbb{R}^{2n}$; matrices $\mathcal{M} \in \mathbb{R}^{2n\times 2n}$, $\jmath \in \mathbb{R}^{2m\times 2n}$, and $\mathcal{K} \in \mathbb{R}^{2m\times 2m}$ are

$$\mathcal{M} = \begin{bmatrix} \mathcal{W} & \mathbf{0}_{n\times n} \\ \mathbf{0}_{n\times n} & Q \end{bmatrix}, \ \jmath = \begin{bmatrix} \mathcal{J}_{\mathrm{L}} & \mathbf{0}_{m\times n} \\ \mathbf{0}_{m\times n} & \mathcal{J}_{\mathrm{R}} \end{bmatrix}, \ \mathcal{K} = \begin{bmatrix} \mathcal{K}_{\mathrm{L}} & \mathbf{0}_{m\times m} \\ \mathbf{0}_{m\times m} & \mathcal{K}_{\mathrm{R}} \end{bmatrix}$$

with matrix $\mathcal{M}$ and vector b being determined by a specific redundancy-resolution scheme. $\mathcal{K}$ is the feedback gain and determined by the actual effect. In actual applications, if $\mathcal{M} = [\mathcal{H}_{\mathrm{L}}, 0; 0, \mathcal{H}_{\mathrm{R}}]$ with $\mathcal{H}$ denoting the inertia matrix and $b = 0$, Eqs. (15)-(18) constitute a minimum-kinetic-energy (MKE) scheme.

If $\mathcal{M}$ is set as an identity matrix and $b = [\lambda(\theta_{\mathrm{L}} - \theta_{\mathrm{L}}(0)); \lambda(\theta_{\mathrm{R}} - \theta_{\mathrm{R}}(0))]$, Eqs. (15)-(18) would be a repetitive motion planning (RMP) scheme. If $\mathcal{M}$ is set as an identity matrix, and $b = 0$, Eqs. (15)-(18) correspond to a minimum-velocity-norm (MVN) scheme. For simplicity and without causing loss of generality, the latter scheme will be used in the following sections.

3 TV-GDD Scheme and Solver

Humanoid robots not only need to perform end-effector tasks, but also desire to act as human would, like emulating human movement and adopting natural-looking postures. Therefore, a corresponding TV-GDD scheme is proposed, and it is solved by a discrete numerical solver.

3.1 TV-GDD Scheme

To enable the robot to generate expected gestures, some joints must be adjusted dynamically according to the tasks with time passing by. For QP methods, the physical limits of a joint are described as two bounds of inequality constraints. Therefore, we can find an appropriate function that can adjust the bounds of desired values. Mathematically, the function which adjusts the joints to the expected states and uses to generate desired gestures dynamically is as follows:

$$\vartheta^{\pm}_{\mathrm{new}}(t) = \vartheta^{\pm} + \frac{\vartheta^{\pm}_{\mathrm{diff}}}{1 + e^{-(t - \mathcal{T}_{\mathrm{SP}})/c_{\mathrm{tuning}}}} \tag{19}$$

where $\vartheta^{\pm}_{\mathrm{diff}} = \vartheta^{\pm}_{\mathrm{goal}} - \vartheta^{\pm}$ with $\vartheta_{\mathrm{goal}} = [\vartheta^{\mathrm{T}}_{\mathrm{goalL}}, \vartheta^{\mathrm{T}}_{\mathrm{goalR}}]^{\mathrm{T}}$ is the expected joint configuration; $0 < c_{\mathrm{tuning}} \leqslant 1$ is a time-tuning parameter, which tunes the variation tendency; $\mathcal{T}_{\mathrm{SP}} = \mathcal{T}_{\mathrm{d}}/N$, with $\mathcal{T}_{\mathrm{d}}$ denoting the task execution duration, and $N \geqslant 1$ influences the proximity between the adjusted values and the initial value/target values. Figure 2 shows that the TV-GDD function (19) can regulate the ith initial joint value $\vartheta^{\pm}_{i}$ into target joint value $\vartheta^{\pm}_{\mathrm{goal}i}$ gradually and smoothly. Without loss of generality, consider $i = 3$ as an example. If $\vartheta^{-}_{\mathrm{goal3}} = \vartheta^{+}_{\mathrm{goal3}} = 5$, the function can adjust the lower/upper limits of the third joint to 5 after a period of time. Given that the robot arms are redundant, kinematic task can still be performed while one or more of the joints is adjusted into an expected configuration.

Consider the TV-GDD function (19), the joint constraint (17) becomes

$$\vartheta^{-}_{\mathrm{new}}(t) \leqslant \vartheta \leqslant \vartheta^{+}_{\mathrm{new}}(t). \tag{20}$$

Given that the redundancy-resolution method is performed at the velocity level, the new joint limit (20) should be formulated using the constraint of $\dot{\vartheta}$ as

$$\nu(\vartheta^{-}_{\mathrm{new}}(t) - \vartheta) \leqslant \dot{\vartheta} \leqslant \nu(\vartheta^{+}_{\mathrm{new}}(t) - \vartheta) \tag{21}$$

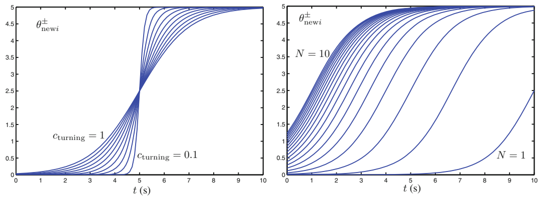

Fig. 2. New joint bounds $\theta^{\pm}_{\text{new}i}$ profiles with different c_{turning} and N ($\theta^{\pm}_{\text{goal}i} = 5$ and $\theta^{\pm}_{i} = 0$). $\theta^{\pm}_{\text{new}i}$ profiles with different c_{turning} ($N = 2$, $\theta^{\pm}_{\text{goal}i} = 5$, and $\theta^{\pm}_{i} = 0$); $\theta^{\pm}_{\text{new}i}$ profiles with different N ($c_{\text{turning}} = 0.9$, $\theta^{\pm}_{\text{goal}i} = 5$ and $\theta^{\pm}_{i} = 0$), respectively.

where parameter $\nu > 0$ is used to scale the feasible region of $\dot{\vartheta}$. In this paper, ν is set as 2. For the ith element, constraints (17) and (18) can be written as

$$\max\{\dot{\vartheta}^{-}_{i}, \nu(\vartheta^{-}_{\text{new}i}(t) - \vartheta_i)\} \leqslant \dot{\vartheta}_i \leqslant \min\{\dot{\vartheta}^{+}_{i}, \nu(\vartheta^{+}_{\text{new}i}(t) - \vartheta_i)\}. \tag{22}$$

With $\zeta^{-}_{\text{new}i}(t) = \max\{\dot{\vartheta}^{-}_{i}, \nu(\vartheta^{-}_{\text{new}i}(t) - \vartheta_i)\}$ and $\zeta^{+}_{\text{new}i}(t) = \min\{\dot{\vartheta}^{+}_{i}, \nu(\vartheta^{+}_{\text{new}i}(t) - \vartheta_i)\}$, the TV-GDD scheme can be formulated as

$$\text{minimize} \quad \dot{\vartheta}^{\mathrm{T}}\mathcal{M}\dot{\vartheta}/2 + b^{\mathrm{T}}\vartheta \tag{23}$$
$$\text{subject to} \quad \jmath(\vartheta)\dot{\vartheta} = \dot{\Upsilon} + k(\vartheta - f(\vartheta)) \tag{24}$$
$$\zeta^{-}_{\text{new}}(t) \leqslant \dot{\vartheta} \leqslant \zeta^{+}_{\text{new}}(t). \tag{25}$$

Kinematic tasks and gestures are performed simultaneously by solving QP problem (23)–(25). Specifically, the gesture model formulated in (19) is integrated into inequality (25) as the bounds, and the kinematic tasks described by the end-effector paths $\dot{r}_{\mathrm{L}}$ and $\dot{r}_{\mathrm{R}}$ are integrated into (5), (9) and (24) as the right-hand sides. Subsequently, the QP-based TV-GDD scheme (23)–(25) is formulated. The scheme is then solved by a discrete QP solver, and the results are further mapped into the robot-controllable value domain. Finally, the control data are sent to the robot controller, which drives the robot to execute the end-effector tasks.

3.2 TV-GDD Scheme Solver

Equations (23)–(25) can be converted to a linear variational inequality (LVI) [12], which is further equivalent to the following linear projection equation:

$$\Phi_{\Omega}(u - (\Gamma u + q)) - u = 0 \tag{26}$$

where $\Phi_{\Omega}(\cdot): \mathbb{R}^{2n+2m} \to \Omega$ is a projection operator, $\Omega = \{u | u^{-} \leqslant u \leqslant u^{+}\} \subset \mathbb{R}^{2n+2m}$, $1_{\iota} := [1, \cdots, 1]^{\mathrm{T}} \in \mathbb{R}^{\iota}$

$$u := \begin{bmatrix} \vartheta \\ \iota \end{bmatrix}, \; u^{+} := \begin{bmatrix} \zeta^{+}_{\text{new}}(t) \\ \omega 1_{\iota} \end{bmatrix} \in \mathbb{R}^{2n+2m}, \; u^{-} := \begin{bmatrix} \zeta^{-}_{\text{new}}(t) \\ -\omega 1_{\iota} \end{bmatrix} \in \mathbb{R}^{2n+2m},$$

$$\Gamma := \begin{bmatrix} \mathcal{M} & -\jmath^{\mathrm{T}}(\vartheta) \\ \jmath(\vartheta) & 0 \end{bmatrix} \in \mathbb{R}^{(2n+2m)\times(2n+2m)}, \; q := \begin{bmatrix} 0 \\ -\dot{\Upsilon} \end{bmatrix} \in \mathbb{R}^{2n+2m}.$$

In addition, $u \in \mathbb{R}^m$ is the primal-dual decision vector, $u^- \in \mathbb{R}^m$ and $u^+ \in \mathbb{R}^m$ are the lower and upper bounds of u, respectively, and ω is set as a sufficiently large value (e.g., in the simulations and experiments, $\varpi = 10^{10}$).

To solve Eq. (26), by defining $\varepsilon(u) := u - \Phi_\Omega(u - (\Gamma u + q))$, the following iterative algorithm causes $\varepsilon(u) \to 0$. Supposing that the initial primal-dual decision variable vector is set as $u^0 \in \mathbb{R}^{2n+2m}$, for iteration number $k = 0, 1, 2, \cdots$, if $u^k \notin \Omega^*$, then [15]

$$u^{k+1} = u^k - \frac{\|\varepsilon(u^k)\|_2^2 \sigma(u^k)}{\|\sigma(u^k)\|_2^2} \tag{27}$$

where $\varepsilon(u^k) = u^k - \Phi_\Omega(u^k - (\Gamma u^k + q))$ and $\sigma(u^k) = (\Gamma^{\mathrm{T}} + I)\varepsilon(u^k)$. For the numerical calculation, $\varepsilon(u^k) = 10^{-5}$.

4 Simulations and Experiments

In this section, the scheme on the physical humanoid robot is performed. The end-effector task is to play a ball game. In the simulations, the initial joints of the left/right arms are $\vartheta_{\mathrm{L}}(0) = [\pi/40, -\pi/10, \pi/30, 0, -131\pi/360, \pi/3, 11\pi/36]^{\mathrm{T}}$ (rad) and $\vartheta_{\mathrm{R}}(0) = [-\pi/40, \pi/10, -\pi/30, \pi, -131\pi/360, \pi/3, \ -25\pi/36]$ (rad), respectively. This task requires the speeds of both hands to be equal to each other; i.e., $\dot{r}_{\mathrm{L}} = \dot{r}_{\mathrm{R}}$. The execution duration is $\mathcal{T}_{\mathrm{d}} = 6\mathcal{T} = 18$ s. The upper/lower limits of the joint velocities of the dual arms are 6 rad/s and −6 rad/s, respectively.

4.1 Synthesized by Pseudoinverse Scheme

For comparison, the pseudoinverse scheme (2)–(3) are applied to the redundancy problem of the dual arms. The end-effector task is to move the ball up, left, down, and then move back. This is to match the latter experiment which tries to move the ball from one cup to another. To illustrate these problems clearly, joint values and velocities of the dual arms synthesized by the pseudoinverse method are shown in Figs. 3 and 4, respectively. Evidently, the generated joint values synthesized by the traditional pseudoinverse scheme (2)–(3) run out of the expected values. That is to say, it cannot accomplish the expected gesture-configuration task. In summary, from the above analysis, the traditional pseudoinverse scheme (2)–(3) is unexpected in actual applications. Specifically, one problem is some joint values or velocities may exceed their physical limits. Another problem is the hands cannot hold the rod stably and the hand gesture would be very strange due to the free rotation of the forearms and wrist.

4.2 Synthesized by TV-GDD Scheme

The TV-GDD scheme is employed to complete the same end-effector task. To keep the forearms and waists moving as little as possible and finally go to an expected gesture, the TV-GDD function (19) is employed. Specifically, $\mathcal{T}_{\mathrm{SP}} =$

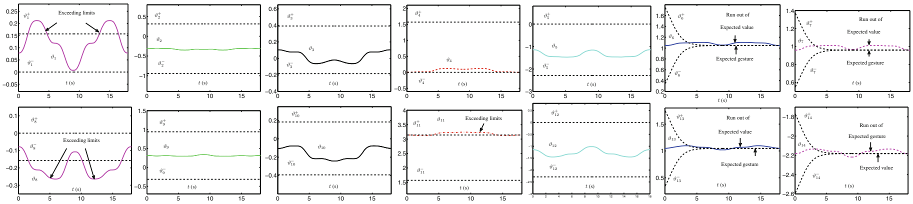

Fig. 3. Dual-arms joint values of the humanoid robot synthesized by pseudoinverse scheme (2)-(3). The ith joint value $\vartheta_{\mathrm{new}i}$ and the bounds $\vartheta^{\pm}_{\mathrm{new}i}$ with $i = 1, 2, ..., 14$.

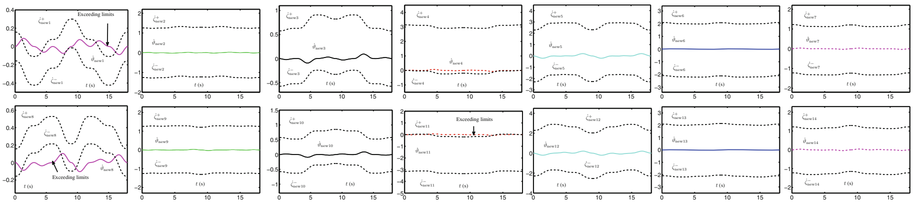

Fig. 4. Joint-velocities synthesized by pseudoinverse scheme (2)-(3) that exceed their limits. The ith joint velocity $\dot{\vartheta}_{\mathrm{new}i}$ subject to $\zeta^{\pm}_{\mathrm{new}i}$ with $i = 1, 2, \ldots, 14$, respectively.

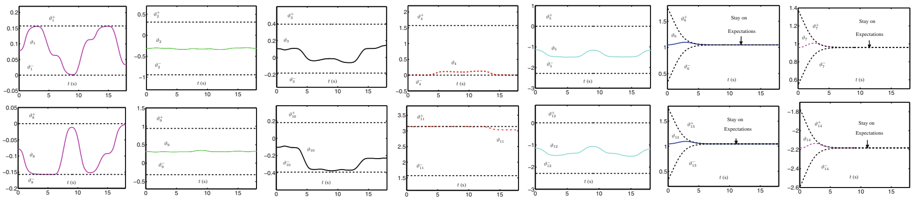

Fig. 5. Dual-arms joint values of the humanoid robot synthesized by TV-GDD scheme (23)-(25). The ith joint value $\vartheta_{\mathrm{new}i}$ subject to $\vartheta^{\pm}_{\mathrm{new}i}$ with $i = 1, 2, \ldots, 14$, respectively.

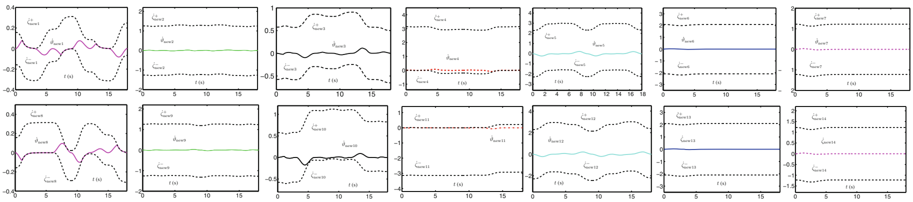

Fig. 6. Dual-arms joint velocities of the humanoid robot synthesized by TV-GDD scheme (23)-(25). The ith joint velocity $\dot{\vartheta}_{\mathrm{new}i}$ subject to $\zeta^{\pm}_{\mathrm{new}i}$ with $i = 1, 2, \ldots, 14$.

0.75 s, $c_{\mathrm{tuning}} = 1$, $\vartheta^{+}_{\mathrm{goalL}} = [9\pi/180, \pi/10, 22.5\pi/180, \pi/2, 0, \pi/3, 55\pi/180]^{\mathrm{T}}$ rad, $\vartheta^{-}_{\mathrm{goalL}} = [0, -54\pi/180, -10.5\pi/180, 0, -131\pi/180, \pi/3,\ 55\pi/180]^{\mathrm{T}}$ rad, $\vartheta^{+}_{\mathrm{goalR}} = [0, 54\pi/180, 10.5\pi/180, \pi, 0, \pi/3,\ -25\pi/36]^{\mathrm{T}}$ rad, $\vartheta^{-}_{\mathrm{goalR}} = [-9\pi/180, -18\pi/180, -22.5\pi/180, \pi/2, -131\pi/180,\ \pi/3, -25\pi/36]^{\mathrm{T}}$ rad.

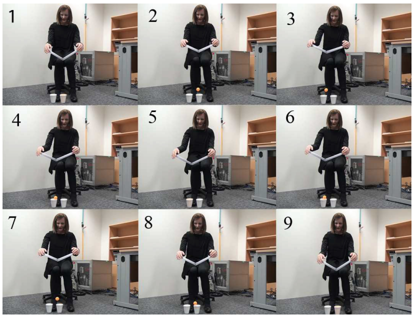

Fig. 7. Snapshots of task execution when the humanoid robot plays with a ball.

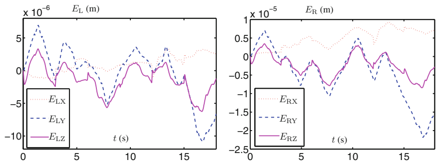

Fig. 8. Positioning-errors of end-effectors (hands) synthesized by the TV-GDD scheme.

To illustrate the effectiveness of the combined time-varying constraint (25) in the scheme, the joint values and velocities of the dual arms during the execution of the task are shown in Figs. 5–6. As shown in Fig. 5, with (19), the upper/lower joint limits tend to overlap after approximately 5 s. This drives joints ϑ_6, ϑ_7, ϑ_{13} and ϑ_{14} to an expected configuration. Furthermore, it also avoids the unexpected rotation of the forearm and wrist at later stages. Figure 6 shows that all the generated joint values never exceed their physical limits and thus that this scheme is applicable. To examine the computational cost, the average computing time within each sampling interval ($\mathcal{T}_{\text{Ave}}$), and the total computing time within each experiment ($\mathcal{T}_{\text{Sum}}$), are measured. While the robot plays with the ball, $\mathcal{T}_{\text{Ave}} = 0.001$ s and $\mathcal{T}_{\text{Sum}} = 1.12$ s, which are both very small compared with the total task execution time $\mathcal{T}_{\text{d}} = 18$ s, thus validating that the computing task can be completed within each sampling interval during the ball-playing experiment. The snapshots during the task execution is shown in Fig. 7. The dual arms lift a yellow ball through a "V" shape stick. It moves the ball along a straight path, places it in another cup, and then move back. During the experiment, the robot moves the ball very well, and keep its hand gesture as expected. Figure 8 shows the positioning-errors of the left/right end-effectors (hands). The errors are measured by the deviations of the generated end-effector trajectories from the desired end-effector paths; i.e., $E = \Upsilon - f(\vartheta)$. It is worth mentioning that the MAE is just 2.1832×10^{-5} m, all AAE are less than 6.2×10^{-6} m, and the RMSE are less than 8.41×10^{-6} m. These tiny errors demonstrate further the accuracy of the TV-GDD scheme in solving the redundancy-resolution problem.

In summary, the above simulations and physical experiment verify that the proposed TV-GDD scheme is effective, accurate and physically realizable.

5 Concluding Remarks

A novel time-varying-constrained scheme for dual-arms motion generation has been proposed and investigated. To generate an expected motion configuration, a time-varying gesture-determined dynamical function is designed. Based on such function, a TV-GDD scheme is derived. To solve such a scheme so as to generate the expected motions, a discrete QP solver is presented and used. These generated optimal solutions are used to control the physical humanoid robot. Both the computer simulations and physical experiments demonstrate the effectiveness and feasibility of the proposed TV-GDD scheme.

Acknowledgments. This work was supported in part by the National Natural Science Foundation under Grants 61603142 and 61633010, the Guangdong Foundation for Distinguished Young Scholars under Grant 2017A030306009, the Science and Technology Program of Guangzhou under Grant 201707010225, the Fundamental Research Funds for Central Universities under Grant 2017MS049.

References

1. Bouyarmane, K., Kheddar, A.: On weight-prioritized multi-task control of humanoid robots. IEEE Trans. Autom. Control **pp**, 1 (2017)
2. Liu, Z., Chen, C., Zhang, Y., Chen, C.L.: Adaptive neural control for dual-arm coordination of humanoid robot with unknown nonlinearities in output mechanism. IEEE Trans. Cybern. **45**, 521 (2015)
3. Xiao, Y., Zhang, Z., Beck, A., Yuan, J., Thalmann, D.: Human-robot interaction by understanding upper body gestures. Presence: Teleoperators Virtual Environ. **23**(2), 133–154 (2014)
4. Shin, S., Kim, C.: Human-like motion generation and control for humanoid's dual arm object manipulation. IEEE Trans. Ind. Electron. **62**, 2265–2276 (2015)
5. Goertz, R.C.: Fundamentals of general purpose remote manipulators. Nucleonics **10**(11), 36–42 (1952)
6. Fletcher, T.: The Undersea Mobot, Nuclear Electronics Laboratory of Hughes Aircraft Company. Technical Report, January 1960
7. Kuindersma, S., Scott, R., Robin, F., Maurice, V.: Optimization-based iocomotion planning, estimation, and control design for the atlas humanoid robot. Auton. Robot. **40**, 429–455 (2016)
8. Lyubova, N., Ivaldi, S., Filliat, D.: From passive to interactive object learning and recognition through self-identification on a humanoid robot. Auton. Robot. **40**, 33–57 (2016)
9. Nunez, J.V., Briseno, A., Rodriguez, D.A., Ibarra, J.M., Rodriguez, V.M.: Explicit analytic solution for inverse kinematics of bioloid humanoid robot. In: Robotics Symposium and Latin American Robotics Symposium, pp. 33–38. IEEE (2012)
10. Wang, J., Li, Y.: Inverse kinematics analysis for the arm of a mobile humanoid robot based on the closed-loop algorithm. In: International Conference on Information and Automation, pp. 516–521. IEEE (2009)

11. Kanoun, O., Lamiraux, F., Wieber, P.-B.: Kinematic control of redundant manipulators: generalizing the task-priority framework to inequality task. IEEE Trans. Robot. **27**(4), 785–792 (2011)
12. Zhang, Z., Zhang, Y.: Acceleration-level cyclic-motion generation of constrained redundant robots tracking different paths. IEEE Trans. Syst. Man Cybern. Part B (Cybern.), **42**(4), 1257–1269 (2012)
13. Zhang, Z., Zhang, Y.: Equivalence of different-level schemes for repetitive motion planning of redundant robots. Acta Autom. Sinica **39**(1), 88–91 (2013)
14. Cheng, F., Chen, T., Sun, Y.: Resolving manipulator redundancy under inequality constraints. IEEE Trans. Robot. Autom. **10**, 65–71 (1994)
15. He, B.: A new method for a class of linear variational inequalities. Math. Program. **66**, 137–144 (1994)